RSC Advances

ROYAL SOCIETY OF CHEMISTRY

www.rsc.org/advances

Cite this: DOI: 10.1039/c0xx00000x

www.rsc.org/xxxxxx

ARTICLE TYPE

Synthesis, structure and photoluminescent properties of a novel color-tunable $Si_{1.92}Al_{0.08}O_{1.08}N_{1.92}$: Eu^{2+}, Tb^{3+}, Sm^{2+}phosphor for ultraviolet white light-emitting diodes

Yichao Wang, Jianyan Ding, Yanyan Li and Yuhua Wang*

Received (in XXX, XXX) Xth XXXXXXXXX 20XX, Accepted Xth XXXXXXXXX 20XX
DOI: 10.1039/b000000x

A novel oxynitride phosphor $Si_{1.92}Al_{0.08}O_{1.08}N_{1.92}$: x%Eu^{2+}, y%Tb^{3+}, z%Sm^{2+} (O-sialon) was successfully synthesized through a high temperature solid-state reaction. The crystal structure, photoluminescent properties and thermal quenching properties have been measured and analyzed. The results indicate that the emission colors can be tuned from blue (0.1716, 0.1508) to green (0.3607, 0.5631) by changing the Eu^{2+}/Tb^{3+} ratio and tuned from white (0.2377, 0.2991) to deep red (0.3573, 0.2231) by changing the Sm^{2+} concentration from 0 to 0.03% in $Si_{1.92}Al_{0.08}O_{1.08}N_{1.92}$: 0.18%$Eu^{2+}$, 1%$Tb^{3+}$, z%$Sm^{2+}$. The energy transfer from Eu^{2+} to Tb^{3+} in $Si_{1.92}Al_{0.08}O_{1.08}N_{1.92}$: Eu^{2+}, Tb^{3+} and the energy transfer from Eu^{2+}/Tb^{3+} to Sm^{2+}in $Si_{1.92}Al_{0.08}O_{1.08}N_{1.92}$: Eu^{2+}, Tb^{3+}, Sm^{2+} have been studied. The energy transfer mechanism of Eu^{2+} to Tb^{3+} is demonstrated to be a dipole–dipole interaction. Their integrated emission intensity at 150 °C all remain 90% of that measured at room temperature. The results indicate that the $Si_{2-n}Al_nO_{1+n}N_{2-n}$: x%Eu^{2+}, y%Tb^{3+}, z%Sm^{2+} phosphor is a very promising candidate for use as a ultraviolet white light-emitting diode phosphor.

1. Introduction

In the field of advanced lighting and displays technology, white light-emitting diodes (WLEDs) have been attracting intense attention due to their high efficiency, compactness, long operational lifetime and energy saving.[1–4]Until now, the commercial WLEDs were achieved by the combination of an InGaN chip with a $Y_3Al_5O_{12}$: Ce^{3+} (YAG:Ce^{3+}) phosphor. However, this kind of WLED exhibits a high correlated color temperature (CCT) and a poor color rendering index due to a lack of the red emission band.[5-7] In order to overcome this problem, the method of blending tricolor (blue, green, red) phosphors upon the UV chips has been employed to realize warm-WLEDs. However, this method also suffers from the problem of low luminescence efficiency and color aberration due to emission reabsorption and different degradation rates of the three primary phosphors.[8-10] It is an urgent task to develop novel single-phased multi-color-emitting phosphors with high chemical and thermal stability for UV WLEDs to avoid the abovementioned problems. A single-composition multi-color-emitting phosphor can be produced by co-doping sensitizers and activators into the same crystalline matrix, using the principle of energy transfer from the sensitizers to the activators**,** such as $Ca_6Y_2Na_2(PO_4)_6F_2$:Eu^{2+}, Mn^{2+},[11] $La_5Si_2BO_{13}$:Ce^{3+}, Mn^{2+},[12] $CaZr(PO_4)_2$:Eu^{2+} /Eu^{3+},[13] Ca_2NaSiO_4F:Ce^{3+}, Eu^{2+}, Tb^{3+},[14] and so on, but there is not an ideal commercial phosphor for this way, so finding new phosphors and investigating energy transfer between different rare earth ions are important things for single-composition multi-color-emitting phosphor.

As far as the sensitizers and activators, the rare earth ions were used for them in most inorganic phosphors because of their abundant emission color.[15-18] It is well known that the Eu^{2+} ions has broad excitation and emission bands with high efficiency due to their spin and orbit allowed 4f–5d electronic transitions.[19] Moreover, the emission color of Eu^{2+} in different hosts has alterable emission peaks, depending on different crystal field splitting resulting from their surrounding ligands.[20,21] The Tb^{3+} ion is regarded as a promising green activator for showing sharp lines at 486, 542, 582 and 619 nm due to $^5D_4 \rightarrow {}^7F_6$, $^5D_4 \rightarrow {}^7F_5$, $^5D_4 \rightarrow {}^7F_4$ and $^5D_4 \rightarrow {}^7F_3$ transitions, respectively. For many materials, in order to have intense Tb^{3+} emission in the phosphor, sensitizers such as Eu^{2+} and Ce^{3+} are needed, since the f–f transitions of Tb^{3+} ion arespin-forbidden.[22,23] Moreover divalent Sm^{2+} has the $4f^6$ electron configuration, which can be excited into the $4f^55d^1$ continuum under irradiation with UV and visible light. The Sm^{2+}-doped phosphors often exhibits efficient deep red emission.[24-26] Compared with other red emission ions (Eu^{3+}, Mn^{2+}, Pr^{3+}) which are usually used for energy transfer, the Sm^{2+} often shows a more wide broadband excitation. This may make

the Sm^{2+} a potential red emission ion for energy transfer.

As for hosts, nitrides and oxynitrides such as $MAlSiN_3$ (M = Ca, Sr),[27, 28, 29] $MYSi_4N_7$ (M = Sr, Ba),[30,31] $MSi_2O_2N_2$ (M = Ca, Sr, Ba),[32, 33] α-SiAlON,[34,35] and β-SiAlON,[36] are good candidates for host materials owing to several merits such as their high chemical, physical stability and low thermal quenching.[37] In the oxynitride or nitride phosphors, β-sialon is well known as a great green phosphor, which has a special structure, derived from β-Si_3N_4 by equivalent substitution of Al–O for Si–N, and the activators are situated into the channel of c direction. The o-sialon is a common and excellent ceramic material in Si-Al-O-N phase diagram which has a similar structure with β-sialon.[38] The structure is derived from Si_2N_2O by equivalent substitution of Al–O for Si–N, which can be written as $Si_{2-n}Al_nO_{1+n}N_{2-n}$. However, the luminescence properties of o-sialon have not been previously investigated. So we chose the o-sialon for the study and synthesize a series of novel oxynitride phosphors $Si_{2-n}Al_nO_{1+n}N_{2-n}$ doped with Eu^{2+}, Tb^{3+} and Sm^{2+}. The crystal structure, thermal quenching and occupation situation of lanthanide ions for the o-sialon were investigated. Their luminescent properties under UV excitation and the energy transfer were studied.

2. Experimental

A series of Eu^{2+}, Tb^{3+}, Sm^{2+} singly and co-doped $Si_{2-n}Al_nO_{1+n}N_{2-n}$ were synthesized by a solid state reaction. The starting materials employed are Si (A.R.), SiO_2 (A.R.), $Al(OH)_3$ (A.R.), Eu_2O_3 (99.99%), Tb_4O_7 (99.99%) and Sm_2O_3 (99.99%). The ingredients were well mixed and sintered in boron nitride (BN) crucibles at 1400°*C* for 2h and subsequently at 1550°C for 4 h in a reducing atmosphere of 20% H_2 –80% N_2.

The phase structures of the obtained samples were characterized by powder X-ray diffraction (XRD) using a Rigaku diffractometer with Ni-filtered Cu Kα radiation. The photoluminescence (PL) and photoluminescence excitation (PLE) spectra were obtained by a FLS-920T fluorescence spectrophotometer equipped with Xe 900 (450 W xenon arc lamp) as the light source. The PL decay curves were measured by a FLS-920 T fluorescence spectrophotometer with an nF900 ns Flashlamp as the light source. All the measurements were performed at room temperature. High-temperature luminescence intensity measurements were carried out by using an aluminum plaque with cartridge heaters; the temperature was measure by thermocouples inside the plaque and controlled by a standard TAP-02 high-temperature fluorescence controller.

3. Results and discussion

3.1 Phase identification and crystal structure

To evaluate the structural parameters of $Si_{1.92}Al_{0.08}O_{1.08}N_{1.92}$: structural refinement was carried out by the material studio program using the Rietveld method. As displayed in Fig. 1(a), the red solid line and black crosses represent the calculated and experimental patterns, respectively. The pink short vertical lines show the Bragg reflection positions of the calculated pattern. The difference between the experimental and calculated results is plotted by the blue line at the bottom. The structural parameters of $Si_{1.96}Al_{0.04}N_{1.96}O_{1.04}$ are used as the initial parameters in the Rietveld analysis.[39] The resulting crystallographic data of

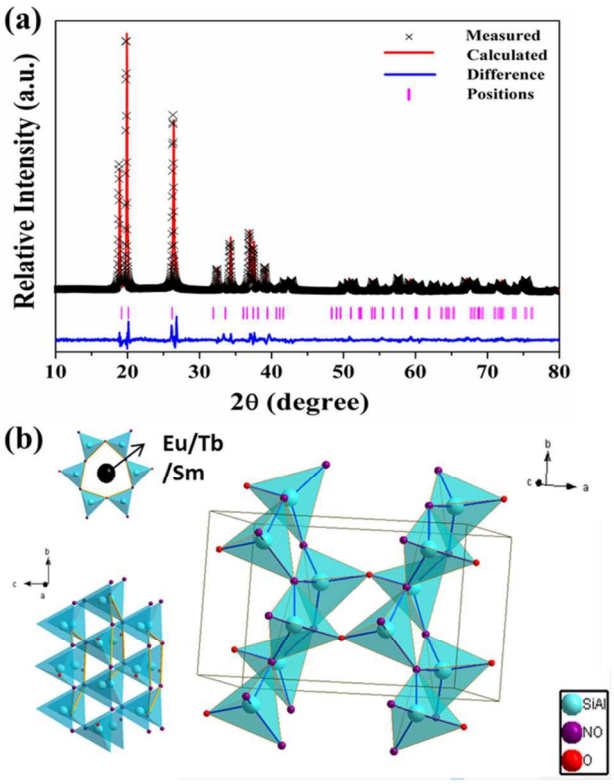

Fig. 1 (a) Rietveld refinement of the powder XRD profile of $Si_{1.92}Al_{0.08}O_{1.08}N_{1.92}$ (b) The crystal structure of $Si_{1.92}Al_{0.08}O_{1.08}N_{1.92}$ and the coordination environment of the activator ions.

$Si_{1.92}Al_{0.08}O_{1.08}N_{1.92}$ is summarized in Table 1. The atomic coordinates and site occupancy fraction (SOF) are presented in the supplementary information (Table S1). All atomic positions and equivalent isotropic displacement parameters were refined converging to the residual factors R_{wp}=13.27%, R_p=9.17%. We can find that the $Si_{1.92}Al_{0.08}O_{1.08}N_{1.92}$ has orthorhombic crystal system (Cmc6 space group) which is similar to the crystal system of $Si_{1.96}Al_{0.04}N_{1.96}O_{1.04}$.

As shown in Fig.1 (b), the $Si_{1.92}Al_{0.08}O_{1.08}N_{1.92}$ comprises a three-dimensional network structure of $(Si,Al)(O,N)_4$ tetrahedra with a continuous and folded channel. The channel was formed by the corner shared connection and it is composed by six-membered ring arraying along the c direction. There are six sites on the six-membered ring. Two of which are only occupied by O^{2-}, the other four can be occupied by O^{2-} or N^{3-}. When the rare earth ions are doped, the coordination environments of the cation sites are not appropriate for them to occupy, because Eu^{2+}(. 1.17 Å, CN = 6; 1.25 Å, CN = 8),Tb^{3+} (0.92 Å, CN = 6; 1.04 Å, CN = 8) and Sm^{2+} (0.96 Å, CN = 6; 1.27 Å, CN = 8) have a larger radius compared with Al^{3+}(0.39 Å, CN = 4) and Si^{4+}(1.17 Å, CN = 6), we think that the rare earth ions could not occupy any sites of cation ions (Al^{3+}, Si^{4+}) in the structure of o-sialon. We can not know the definite position of the rare earth ions in $Si_{1.92}Al_{0.08}O_{1.08}N_{1.92}$, however because the $Si_{1.92}Al_{0.08}O_{1.08}N_{1.92}$ have the similar structure composition of $(Si,Al)(O,N)_4$ tetrahedra and the analogical channel composed by six-membered ring with β-sialon, we can obtain some enlightenment from the rare earth ions in β-sialon. Lin Gan et al. describe detailedly and

demonstrate the position of Ce in β-SiAlON using an atom-resolved Cs-corrected scanning transmission electron microscope. The Ce^{3+} have two sites which are in the c-projected structural channels coordinated with six and nine N (O) atoms. We can reasonably infer that the positions of rare earth ions in $Si_{1.92}Al_{0.08}O_{1.08}N_{1.92}$ are also in the interspace or channel and there are several coordination environments around Eu^{2+} ions.

Table 1 Crystal structural data and lattice parameters

Formula	$Si_{1.92}Al_{0.08}O_{1.08}N_{1.92}$
Crystal System	Orthorhombic
Space group	Cmc21(36)
a/ Å	8.8901
b/ Å	5.5002
c/ Å	4.8545
α/°	90
β/°	90
γ/°	90
R_{wp}	13.27%
R_p	9.17%

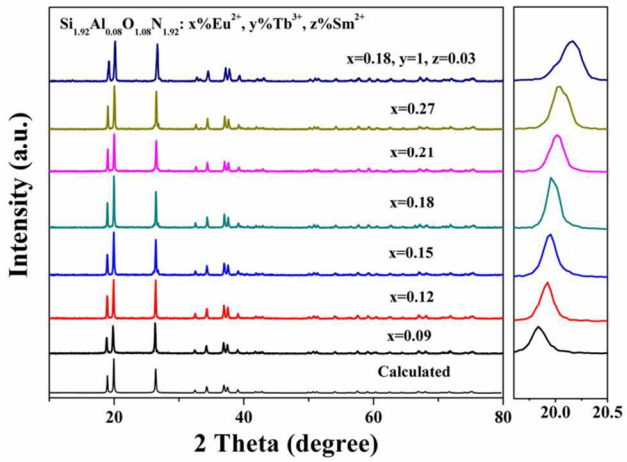

Fig. 2 The XRD patterns of the $Si_{1.92}Al_{0.08}O_{1.08}N_{1.92}$: $x\%Eu^{2+}$ ($0.09 \le x \le 0.27$) and $Si_{1.92}Al_{0.08}O_{1.08}N_{1.92}$: $18\%Eu^{2+}$, $1\%Tb^{3+}$, $0.03\%Sm^{2+}$ samples.

Fig. 2 shows the XRD patterns of the obtained $Si_{1.92}Al_{0.08}O_{1.08}N_{1.92}$: $x\%Eu^{2+}$ ($0.09 \le x \le 0.27$) and $Si_{1.92}Al_{0.08}O_{1.08}N_{1.92}$: $18\%Eu^{2+}$, $1\%Tb^{3+}$, $0.03\%Sm^{2+}$ phosphors. When the diffraction data are compared with the simulated patterns, it is found that all the positions and relative intensities are in good agreement with the calculated and no impurity phase is detected. The results show that there is no detectable impurity phase presented when doping Eu^{2+}, Tb^{3+} and Sm^{2+} ions.

3.2 Photoluminescent properties

3.2.1 Photoluminescent properties of $Si_{2-n}Al_nO_{1+n}N_{2-n}$: Eu^{2+}.

Considering that there is different environment in the c channel and the Eu^{2+} ions are sensitive to their surrounding ligands. The Gaussian fitting was used for analysis. The emission spectrum of $Si_{1.92}Al_{0.08}O_{1.08}N_{1.92}$: $0.18\%Eu^{2+}$ under 340nm excitation and its Gaussian fitting are shown in Fig. 3(a). The emission spectrum can be decomposed into three components with the maxima at 400(M1), 450(M2), and 500(M3). The three emission bands are assigned to the $4f^65d^1 \rightarrow 4f^7$ transition of Eu^{2+}in different coordination environments. The appearance of the three peaks results from that the different proportion of oxygen and nitrogen

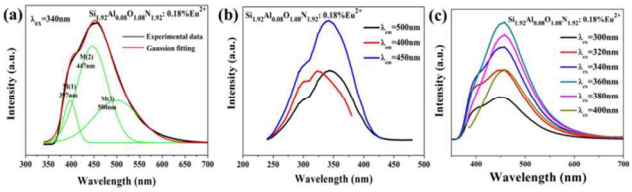

Fig. 3 (a) The experimental data and Gaussian fitting of the emission spectrum $Si_{1.92}Al_{0.08}O_{1.08}N_{1.92}$:$0.18\%Eu^{2+}$ monitored at 340nm.(b)The emission spectra of $Si_{2-n}Al_nO_{1+n}N_{2-n}$:$0.18\%Eu^{2+}$ (z=0.032, 0.048, 0.064, 0.08). (b)The excitation spectra of $Si_{1.92}Al_{0.08}O_{1.08}N_{1.92}$:$0.18\%Eu^{2+}$ monitored at different emissions (400nm, 450nm, 500nm).(c)The emission spectra of $Si_{1.92}Al_{0.08}O_{1.08}N_{1.92}$:$0.18\%Eu^{2+}$ under different excitation wavelengths (300nm, 320nm, 340nm, 360nm, 380nm, 400nm).

around the Eu^{2+} ions forms the different coordination environments. While increasing the rate of O/N, the size of the channel becomes larger, which will reduce the crystal field strength and make the emission band shift to shorter wavelength.

In order to further demonstrate there are different luminescent centers for $Si_{1.92}Al_{0.08}O_{1.08}N_{1.92}$: Eu^{2+}, the excitation spectra monitored at different wavelengths and emission spectra of $Si_{1.92}Al_{0.08}O_{1.08}N_{1.92}$: $0.18\%Eu^{2+}$ are shown in Fig. 3(b) and 3(c). When monitoring different emission peaks, we can observe different excitation peaks, and by changing the excitation wavelengths, the shapes of the emission spectra have different

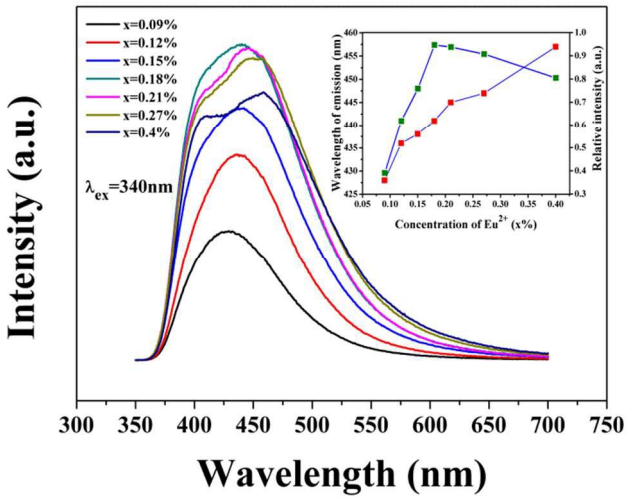

Fig. 4 The emission spectra of $Si_{1.92}Al_{0.08}O_{1.08}N_{1.92}$: $x\%Eu^{2+}$ ($0.09 \le x \le 0.4$). The inset shows the relationship between the emission intensity or the emission peak of Eu^{2+} ions and the doped Eu^{2+} content.

peak patterns. The results further prove that the $Si_{1.92}Al_{0.08}O_{1.08}N_{1.92}$ have more than one position for Eu^{2+} to occupy.

The influence of the Eu^{2+} concentration on the luminescent properties was investigated by varying the Eu^{2+} concentration between 0.09% and 0.4%. The emission spectra of $Si_{1.92}Al_{0.08}O_{1.08}N_{1.92}$ with varied Eu^{2+} concentrations under excitation at 340 nm are given in Fig. 4. As the concentration of Eu^{2+} increased, the luminescence intensity increased and reached a maximum at x= 0.007. When the Eu^{2+} concentration exceeded 0.007, concentration quenching occurred. Meanwhile, the emission peak positions of the $Si_{1.92}Al_{0.08}O_{1.08}N_{1.92}$: xEu^{2+}

phosphors shift from 427 nm to 458 nm as the Eu^{2+} concentration increases. The red shift of the emission peak can be ascribed to two reasons. First, when the Eu^{2+} concentration was changed, the shapes of emission spectra are different. So we infer that the intensity of three sites have inequable change degree relative to the same variation of Eu^{2+} concentration, which can make different peak positions. Second, From the Fig. 2, we observe that the shift toward largeangle of the diffraction position was happened with the increasing of Eu^{2+}. Due to the Bragg equation, the lattice constant become smaller with the increasing of Eu^{2+}. The red-shifting behavior of the emission band can be explained in terms of the Eu^{2+} ions experiencing a strengthening of the crystal field strength caused by increasing Eu^{2+} concentration due to the shrinkage of the lattice.

3.2.2 Luminescence properties of $Si_{1.92}Al_{0.08}O_{1.08}N_{1.92}:Eu^{2+}$, Tb^{3+}, Sm^{2+}.

Fig. 5(a) shows the excitation and emission spectra of $Si_{1.92}Al_{0.08}O_{1.08}N_{1.92}$: 0.18%$Eu^{2+}$, and Fig. 5(b) displays the excitation and emission spectra of $Si_{1.92}Al_{0.08}O_{1.08}N_{1.92}$: 1%$Tb^{3+}$. Monitored at 542nm, the excitation spectrum of Tb^{3+} contains an intense broad band at 250nm, which is attributed to the allowed transition of the Tb^{3+} from the ground state ($^7F_6$) to excited states of the $4f^75d^1$configuration. There are also many peaks located at 284, 295, 303, 318, 338, 355, 379, 486nm in the excitation spectrum, which are due to the various forbidden 4f→4f transitions of Tb^{3+} ions.[40,41] From the emission spectrum excited at 250nm, it can be seen that the emission spectrum is dominated by the characteristic green emission $^5D_4\rightarrow{}^7F_5$ (542nm) transitions of Tb^{3+}, and the emission also has some weaker peaks due to the $^5D_4\rightarrow{}^7F_6$ (486 nm),$^5D_4\rightarrow{}^7F_4$ (587nm) and $^5D_4\rightarrow{}^7F_3$ (619nm) of Tb^{3+}.

A considerable spectral overlap between the PL spectrum of $Si_{1.92}Al_{0.08}O_{1.08}N_{1.92}$: 0.18%$Eu^{2+}$ and the PLE spectrum of $Si_{1.92}Al_{0.08}O_{1.08}N_{1.92}$: 1%$Tb^{3+}$ were observed. This implies that the energy transfer from Eu^{2+} to Tb^{3+} would be highly expected in Eu^{2+} and Tb^{3+} co-doped $Si_{1.92}Al_{0.08}O_{1.08}N_{1.92}$. Fig. 5(c) shows the PL and PLE spectra of $Si_{1.92}Al_{0.08}O_{1.08}N_{1.92}$: 0.18%$Eu^{2+}$, 1%$Tb^{3+}$. At the excitation of 340nm, the phosphor shows blue emission of the Eu^{2+} ions and green emission of the Tb^{3+} ions. Monitored at 542 nm, the excitation spectrum shows a broad band, which has a similar shape with the PLE spectrum of $Si_{1.92}Al_{0.08}O_{1.08}N_{1.92}$: 0.18%$Eu^{2+}$. This indicates the occurrence of an energy transfer from Eu^{2+} to Tb^{3+}, and the doped of Eu^{2+} enhanced the efficient of Tb^{3+} under the excitation at 340nm.

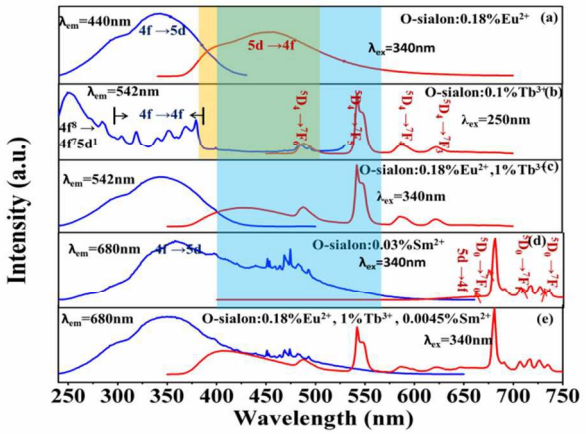

Fig. 5 Emission spectra (right) and excitation spectra (left) of $Si_{1.92}Al_{0.08}O_{1.08}N_{1.92}$: 0.18%$Eu^{2+}$ (a), $Si_{1.92}Al_{0.08}O_{1.08}N_{1.92}$: 1%$Tb^{3+}$ (b), $Si_{1.92}Al_{0.08}O_{1.08}N_{1.92}$: 0.18%$Eu^{2+}$, 1%$Tb^{3+}$ (c), $Si_{1.92}Al_{0.08}O_{1.08}N_{1.92}$: 0.03%$Sm^{2+}$ (d), and $Si_{1.92}Al_{0.08}O_{1.08}N_{1.92}$: 0.18%$Eu^{2+}$, 1%$Tb^{3+}$, 0.0045%$Sm^{2+}$ (e) samples.

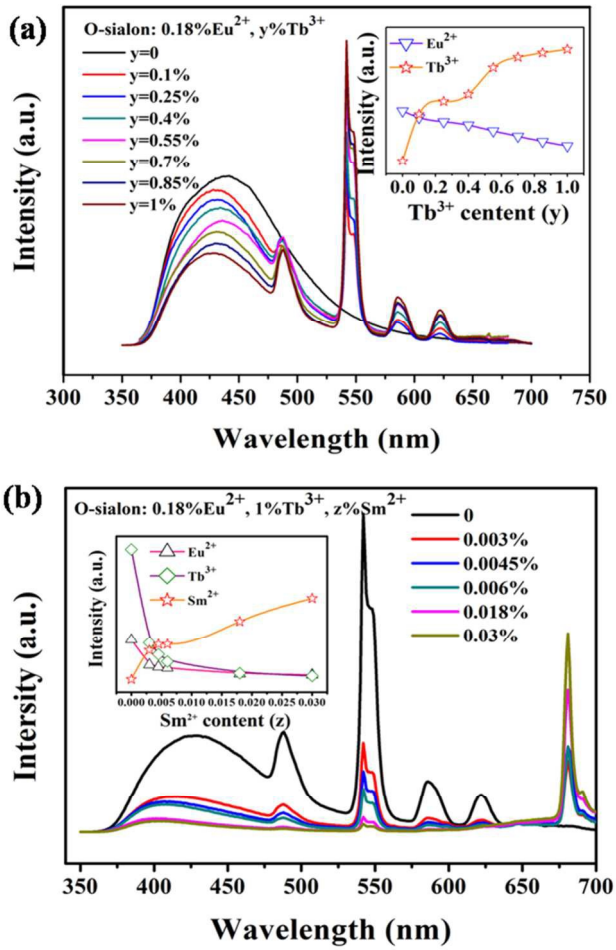

Fig. 6(a) The emission spectra of $Si_{1.92}Al_{0.08}O_{1.08}N_{1.92}$: 0.18%$Eu^{2+}$, y%$Tb^{3+}$ ($0 \le y \le 1$). The inset shows the relationship between the emission intensity of Eu^{2+} and Tb^{3+} ions and the doped Tb^{3+} content. (b)The emission spectra of $Si_{1.92}Al_{0.08}O_{1.08}N_{1.92}$: 0.18%$Eu^{2+}$, 1%$Tb^{3+}$, z%$Sm^{2+}$ ($0 \le z \le 0.03$). The inset shows the relationship between the emission intensity of Eu^{2+}, Tb^{3+} and Sm^{2+} ions and the doped Sm^{2+} content.

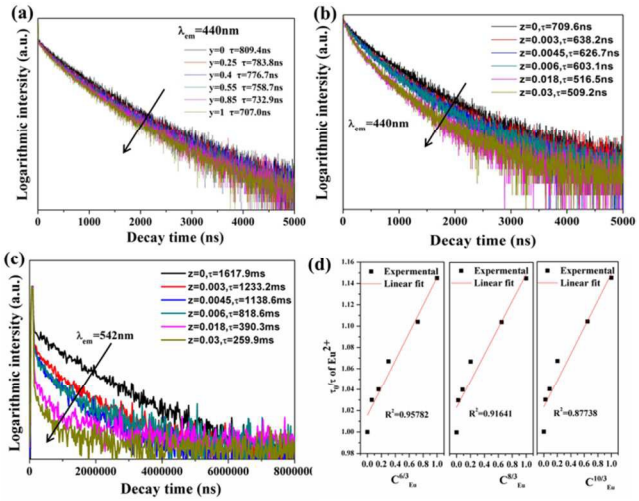

Fig. 7 (a) Decay curves of Eu^{2+} in $Si_{1.92}Al_{0.08}O_{1.08}N_{1.92}$: 0.18%$Eu^{2+}$, y%$Tb^{3+}$ ($0 \le y \le 1$) displayed on a logarithmic intensity scale (excited at 340 nm, monitored at 440 nm). (b) Decay curves of Eu^{2+} in $Si_{1.92}Al_{0.08}O_{1.08}N_{1.92}$: 0.18%$Eu^{2+}$, 1%$Tb^{3+}$, z%$Sm^{2+}$ ($0 \le z \le 0.03$) displayed on a logarithmic intensity scale (excited at 340 nm, monitored at 440 nm). (c) Decay curves of Tb^{3+} in $Si_{1.92}Al_{0.08}O_{1.08}N_{1.92}$:0.18%$Eu^{2+}$, 1%$Tb^{3+}$, z%$Sm^{2+}$ ($0 \le z \le 0.03$) displayed on a logarithmic intensity scale (excited at 340 nm, monitored at 542 nm).(d)The dependence of I_0 /I of Eu^{2+} on $C^{6/3}$, $C^{8/3}$ and $C^{10/3}$in $Si_{1.92}Al_{0.08}O_{1.08}N_{1.92}$: 0.18%$Eu^{2+}$, y%$Tb^{3+}$ ($0 \le y \le 1$).

Fig.5(d) displays the excitation and emission spectra of $Si_{1.92}Al_{0.08}O_{1.08}N_{1.92}$: 0.03%$Sm^{2+}$. The emission spectrum under 340nm excitation of Sm^{2+} doped $Si_{1.92}Al_{0.08}O_{1.08}N_{1.92}$ shows the sharp emission lines at 680nm, 710nm and 730nm of Sm^{2+} ions overlapped on the weak broad emission between 600 and 750nm, the sharp emission can be attributed to $^5D_0 \rightarrow {}^7F_j$(j=0,1,2) transition and the broad band can be attributed to 5d→4f transition of Sm^{2+}. When monitored at 680 nm the excitation spectrum shows a wide range from 250nm to 600nm consisting of two broad bands with maxima at 360 and 470 nm, respectively, the bands can be attributed to transitions from the $4f^6$ ground state to the $4f^55d^1$ excited states of Sm^{2+}. It can be find that the excitation spectrum of $Si_{1.92}Al_{0.08}O_{1.08}N_{1.92}$: 0.03%$Sm^{2+}$ has an obvious spectral overlap with the emission spectrum of $Si_{1.92}Al_{0.08}O_{1.08}N_{1.92}$: 0.18%$Eu^{2+}$ and $Si_{1.92}Al_{0.08}O_{1.08}N_{1.92}$: 1%$Tb^{3+}$. This implies that the energy transfer from Eu^{2+}, Tb^{3+} to Sm^{2+} maybe happened in the Eu^{2+}, Tb^{3+} and Sm^{2+}co-doped $Si_{1.92}Al_{0.08}O_{1.08}N_{1.92}$. Fig. 5(e) shows the excitation and emission spectra of $Si_{1.92}Al_{0.08}O_{1.08}N_{1.92}$: 0.18%$Eu^{2+}$, 1%$Tb^{3+}$, 0.0045%$Sm^{2+}$, which also have a wide broad band excitation from 250 to 600nm monitoring at 680 nm. Comparing with the $Si_{1.92}Al_{0.08}O_{1.08}N_{1.92}$: Sm^{2+}, it has a stronger absorption at 250-400nm and the shape of this range is alike to the excitation spectra of $Si_{1.92}Al_{0.08}O_{1.08}N_{1.92}$: 0.18%$Eu^{2+}$, 1%$Tb^{3+}$. So we infer that the energy transfer could happen from Eu^{2+}/Tb^{3+} to Sm^{2+}.

In order to further understand the energy transfer between the Eu^{2+}, Tb^{3+} and Sm^{2+} ions. A series of $Si_{1.92}Al_{0.08}O_{1.08}N_{1.92}$: 0.18%$Eu^{2+}$, y%$Tb^{3+}$, z%$Sm^{2+}$ samples were prepared for the investigation. Fig.6(a) shows the emission spectra of $Si_{1.92}Al_{0.08}O_{1.08}N_{1.92}$: 0.18%$Eu^{2+}$, y%$Tb^{3+}$ ($0 \le y \le 1$) and the variation of the emission intensity of Eu^{2+} and Tb^{3+} ions excited at 340 nm. The Eu^{2+} content was fixed at 0.18% which is the optimal content, while the Tb^{3+} content changes from 0 to 1%. As can be seen, the intensity of the emission spectra of the Eu^{2+} ions decreases monotonically with an increase in the Tb^{3+} doping content, whereas the intensity of the Tb^{3+} emission obviously increases. In addition, the emission peak positions have a blue shift with the increasing of Tb^{3+} because of the different energy transfer efficiencies for the three lattice site These demonstrate the existence of the energy transfer from Eu^{2+} to Tb^{3+}. Fig. 6(b) shows the emission spectra of $Si_{1.92}Al_{0.08}O_{1.08}N_{1.92}$: 0.18%$Eu^{2+}$, 1%$Tb^{3+}$, z%$Sm^{2+}$ ($0 \le z \le 0.03$) and the variation of the emission intensity of Eu^{2+}, Tb^{3+} and Sm^{2+} ions excited at 340 nm. As can be seen, the intensity of the emission spectra of the Eu^{2+} ions and Tb^{3+} decreases monotonically and the intensity of the Sm^{2+} emission spectra obviously increases with the increasing of Sm^{2+}concentration.This proves that the energy transfer from Eu^{2+}or/and $Tb^{3+}$to Sm^{2+} is existent.

To provide further evidence of the phenomenon that the energy transfer from the Eu^{2+} to the Tb^{3+} ions and Eu^{2+}/$Tb^{3+}$to the Sm^{2+} ions occurs in the $Si_{1.92}Al_{0.08}O_{1.08}N_{1.92}$ host, some fluorescence decay curves were measured. Fig. 7(a) shows the PL decay curves of Eu^{2+} in the $Si_{1.92}Al_{0.08}O_{1.08}N_{1.92}$: 0.18%$Eu^{2+}$, y%$Tb^{3+}$ ($0 \leqslant y \leqslant 1$). Fig 7(b) and 7(c) shows the PL decay curves of Eu^{2+} and Tb^{3+} in the $Si_{1.92}Al_{0.08}O_{1.08}N_{1.92}$: 0.18%$Eu^{2+}$, 1%$Tb^{3+}$, z%$Sm^{2+}$ ($0 \le z \le 0.03$) samples. The fluorescence of them all tends to be a non-exponential function with increasing the Tb^{3+} or Sm^{2+} concentration. The decay process of these samples are characterized by an average lifetime, τ， which can be calculated using equation (1) [42, 43] as follows：

$$\tau = \frac{\int_0^{+\infty} I(t)tdt}{\int_0^{+\infty} I(t)dt} \quad (1)$$

where I(t) is the luminous intensity at time t. On the basis of equation (1), the lifetimes are listed in the Fig.7. We can find that the lifetimes of Eu^{2+} and Tb^{3+} in the $Si_{1.92}Al_{0.08}O_{1.08}N_{1.92}$: 0.18%$Eu^{2+}$, y%$Tb^{3+}$ and $Si_{1.92}Al_{0.08}O_{1.08}N_{1.92}$: 0.18%$Eu^{2+}$, 1%$Tb^{3+}$, z%$Sm^{2+}$ all have a decreasing trend with the increasing of activators. This demonstrates that the energy transfers from $Eu^{2+} \rightarrow Tb^{3+}$ and Eu^{2+}, $Tb^{3+} \rightarrow Sm^{2+}$ are existent.

Energy transfer efficiency η between the Eu^{2+} and Tb^{3+} ions was also obtained from the decay lifetime by using the equation(2):[43-45]

$$\eta = 1 - \frac{\tau_s}{\tau_0} \quad (2)$$

The τ and τ_0 are the lifetimes of sensitizer (Eu^{2+}) ion with and without the presence of activator (Tb^{3+}). The η are calculated to be 0, 0.032, 0.041, 0.063, 0.096 and 0.126 with y=0, 0.05, 0.4, 0.55, 0.85 and 0.1. In general, energy transfer from the sensitizer to the activator in a phosphor may take place via a multipolar interaction or an exchange interaction. This can be evaluated according to the Dexter's theories, [46-48] as given in the following equation(3):

$$\eta_0/\eta \propto C^{n/3} \quad (3)$$

Where η_0 and η are the luminescence quantum of Eu^{2+} in the absence and presence of Tb^{3+} and C is the concentration of Tb^{3+}. When n = 6, 8, and 10, it corresponds to dipole–dipole, dipole–quadrupole, and quadrupole–quadrupole interactions. The value of η_0/η can be estimated approximately from the correlated lifetime ratio (τ_0/τ), thus equation can be changed as follows:

$$\tau_0/\tau \propto C^{n/3} \quad (4)$$

As shown in Fig.7d, this clearly indicates a better fitting result for $C^{6/3}$ compared with the others through the linear fitting. This indicates that the dipole–dipole interaction is mainly responsible for the energy transfer from the Eu^{2+} to the Tb^{3+} ions.

The corresponding energy levels scheme and energy transfer in the $Si_{1.92}Al_{0.08}O_{1.08}N_{1.92}$:0.18%$Eu^{2+}$, y%Tb^{3+}, z%Sm^{2+} upon excitation with UV radiation is illustrated in Fig. 8.The energy transfer behavior between Eu^{2+}, Tb^{3+} and Sm^{2+} ions can be ascribed to the similar value of energy level of the excited 5d state of Eu^{2+}, the ^5D_j (j=3, 4) of Tb^{3+}ions, and the excited 5d state of Sm^{2+}. The energy transfer process can be divided into four parts. The first part is the excitation and the emission of Eu^{2+}. When the Eu^{2+} ions are excited by the UV light, the electron is pumped to the 5d level, and then it relaxes to the lowest 5d crystal field splitting state, and then a blue emission appears owing to the transition from 5d to 4f level.

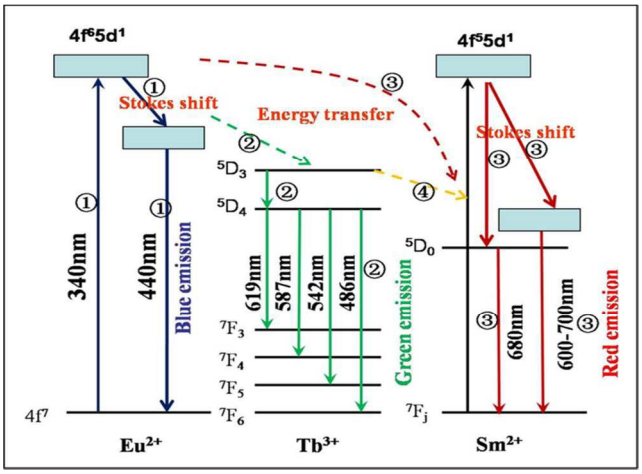

Fig. 8 The energy level diagram and the energy transition schematic diagram of Eu^{2+}, Tb^{3+} and Sm^{2+} in $Si_{1.92}Al_{0.08}O_{1.08}N_{1.92}$: Eu^{2+}, Tb^{3+}, Sm^{2+}.

The second part is the energy transfer from Eu^{2+} to Tb^{3+}. An energy transfer process takes place from the 5d state of Eu^{2+} to $^5D_3$ of Tb^{3+}, which relaxes to levels $^5D_4$ later. Then the excited Tb^{3+} relaxes to the ^7F_j (j=3, 4, 5, 6) levels non-radioactively and gives the green characteristic emission of Tb^{3+}. The third part is the energy transfer from Eu^{2+} to Sm^{2+}. An energy transfer process takes place from the 5d state of Eu^{2+} to 5d state of Sm^{2+}, and then it relaxes to the lowest 5d crystal field splitting state or the $^5D_0$ of Sm^{2+}. And then the sharp emission of $^5D_0 \rightarrow {}^7F_0$ occurs with the weak broad band 5d→4f emission. The fourth part is the energy transfer from Tb^{3+} to Sm^{2+}. An energy transfer process takes place from $^5D_3$ or $^5D_4$ of Tb^{3+} to 5d of Sm^{2+}, and then it gives the emission processes of Sm^{2+} similar to the third part.

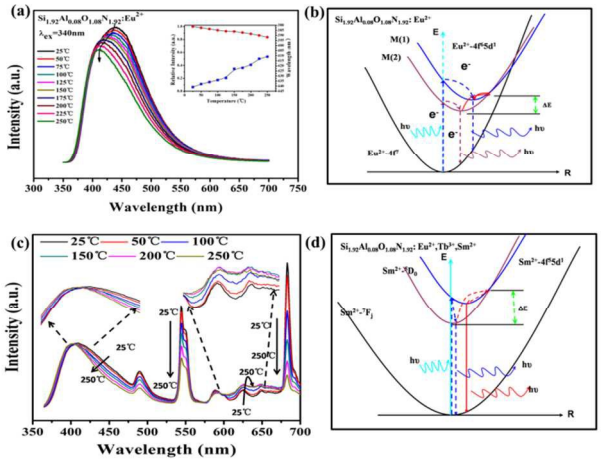

Fig. 9 (a) Temperature dependence of emission intensity of $Si_{1.92}Al_{0.08}O_{1.08}N_{1.92}$: 0.18%$Eu^{2+}$. (b) The schematic configurational coordinate diagrams that present possible mechanisms of temperature-dependent emission for $Si_{1.92}Al_{0.08}O_{1.08}N_{1.92}$: 0.18%$Eu^{2+}$. (c) Temperature dependence of emission intensity of Decay curves of Eu^{2+} in $Si_{1.92}Al_{0.08}O_{1.08}N_{1.92}$: 0.18%$Eu^{2+}$, 1%$Tb^{3+}$, 0.003%$Sm^{2+}$ (b) The schematic configurational coordinate diagrams that present possible mechanisms of temperature-dependent emission for $Si_{1.92}Al_{0.08}O_{1.08}N_{1.92}$: 0.18%$Eu^{2+}$, 1%$Tb^{3+}$, 0.003%$Sm^{2+}$.

3.3 Temperature-dependent PL properties

Thermal quenching is one of the important technological parameters for phosphors used in UV WLEDs. Fig.9 (a) shows the temperature dependence of luminescence for $Si_{1.92}Al_{0.08}O_{1.08}N_{1.92}$: 0.18%$Eu^{2+}$ under 340nm excitation. The emission intensity is about 92% at 150℃, and 84% at 250℃. The shape of the emission spectra shows a blue-shift with increasing temperature due to the thermally active phonon assisted excitation from a lower energy sublevel to a high energy sublevel in the excited state of Eu^{2+}.As shown in Fig.9 (b), At higher temperatures, electrons at lower excited levels (M(2))could jump to higher excited levels(M(1)), assisted by thermal phonons. This makes the result that when increasing temperature the blue shift of emission peak takes place. The energy transfer from M(2) to M(1) can occur by non-radiative relaxation. The temperature dependence of the integrated emission intensity of $Si_{1.92}Al_{0.08}O_{1.08}N_{1.92}$: 0.18%$Eu^{2+}$, 1%$Tb^{3+}$, 0.003%$Sm^{2+}$ is presented in the Fig.9(c). The integrated emission intensity at 150 and 250 °C remains about 90% and 78%. It can be noted that the emission intensity of Sm^{2+} increases for 580-670 nm wavelength. The phenomenon also appeared in the β-sialon: Sm^{2+} and can be rationalized in terms of the energy transfer from $^5D_0$ to $4f^55d^1$.[49] As shown in Fig. 9(d), in $Si_{1.92}Al_{0.08}O_{1.08}N_{1.92}$: 0.18%$Eu^{2+}$, 1%$Tb^{3+}$, 0.003%$Sm^{2+}$ sample, the $4f^55d^1$ state is located at higher energy than the $^5D_0$ state, so at higher temperatures, electrons at lower excited levels ($^5D_0$) could jump to higher excited levels ($4f^55d^1$), resulting in the increase of intensity of $Sm^{2+}$from 600 nm to 670 nm in the range of 25–150 ℃.

3.4 CIE coordinates and quantum efficiency of $Si_{1.92}Al_{0.08}O_{1.08}N_{1.92}$: Eu^{2+}, Tb^{3+}, Sm^{2+}

Fig. 10 shows the variation of the Commission International deL'Eclairage (CIE) chromaticity coordinates of the $Si_{1.92}Al_{0.08}O_{1.08}N_{1.92}$: 0.18%$Eu^{2+}$ (1%Tb^{3+} or 0.03%Sm^{2+}), $Si_{1.92}Al_{0.08}O_{1.08}N_{1.92}$: 0.18%$Eu^{2+}$, y%$Tb^{3+}$ and $Si_{1.92}Al_{0.08}O_{1.08}N_{1.92}$: 0.18%$Eu^{2+}$, 1%$Tb^{3+}$, z%$Sm^{2+}$ under

excitation at 365 nm. The CIE coordinates are calculated and summarized in the supplementary information (Table S2). The results indicate that we can get blue green red and even white emission light and the emission light can be modulated from blue to green with increasing the doping content of Tb^{3+} ions. And the Sm^{2+} can add the red compositions in the $Si_{1.92}Al_{0.08}O_{1.08}N_{1.92}$: 0.18%$Eu^{2+}$, 1%$Tb^{3+}$, making the colors of samples change from white to deep red. So the color can be tunable in a wide range for the $Si_{1.92}Al_{0.08}O_{1.08}N_{1.92}$: 18%$Eu^{2+}$, y%$Tb^{3+}$, z%$Sm^{2+}$. For an evaluation of the luminescence efficiency, the QEs of our phosphors are estimated. The QE of $Si_{1.92}Al_{0.08}O_{1.08}N_{1.92}$: 0.18%$Eu^{2+}$ under 340 nm is measured to be 59.5% at room temperature and the QE of $Si_{1.92}Al_{0.08}O_{1.08}N_{1.92}$: 0.18%$Eu^{2+}$, 1%$Tb^{3+}$, 0.003%$Sm^{2+}$ under 340nm is measured to be 32.8%.

4. Conclusions

In summary, A novel oxynitride phosphors $Si_{2-n}Al_nO_{1+n}N_{2-n}$: x%Eu^{2+}, y%Tb^{3+}, z%Sm^{2+} was synthesized successfully via a solid state reaction and the crystal structure was refined. There are three different crystalline sites for the lanthanide ions. The Eu^{2+}, Tb^{3+} and Sm^{2+} singly-doped $Si_{1.92}Al_{0.08}O_{1.08}N_{1.92}$ respectively show a blue, a green and a deep red emission. It was demonstrated that the energy transfer from Eu^{2+} to Tb^{3+}, Eu^{2+} to Sm^{2+} and Tb^{3+} to Sm^{2+} are subsistent in the $Si_{2-n}Al_nO_{1+n}N_{2-n}$: x%Eu^{2+}, y%Tb^{3+}, z%Sm^{2+}. The change of the color for $Si_{2-n}Al_nO_{1+n}N_{2-n}$: x%Eu^{2+}, y%Tb^{3+}, z%Sm^{2+} in a wide range was successfully realized through the energy transfer. The thermal stabilities of them have a great performance, the blue shift and the increasing of the emission intensity along with the rising of temperature were also investigated. In conclusion, the novel color-tunable$Si_{2-n}Al_nO_{1+n}N_{2-n}$: x%Eu^{2+}, y%Tb^{3+}, z%Sm^{2+} phosphors are expected to have promising applications in UV WLEDs.

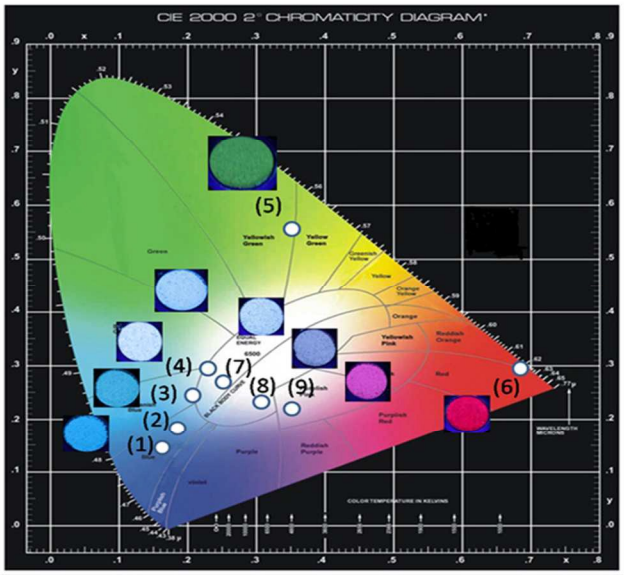

Fig. 10 CIE chromaticity diagram for $Si_{1.92}Al_{0.08}O_{1.08}N_{1.92}$: x%$Eu^{2+}$, y%$Tb^{3+}$, z%$Sm^{2+}$ excited at 340 nm.

Acknowledgements

We acknowledge the financial support from the National Science Foundation under grant No. 51202099 and grant No.51372105, and the Doctoral Program of Higher Education under grant No. 20120211130003, and the State Key Laboratory on Integrated Optoelectronics under grant No.IOSKL2013KF15.

Notes and references

**Key Laboratory for Special Function Materials and Structural Design of the Ministry of Education, School of Physical Science and Technology, Lanzhou University, Lanzhou,730000, China. E-mail: wyh@lzu.edu.cn; Fax: +86-931-8913554; Tel: +86-931-8912772*

1 R. J. Xie, N. Hirosaki, M. Mitomo, K. Sakuma and N. Kiumra, Appl. Phys. Lett., 2006, 89, 241103.
2 J. S. Kim, P. E. Jeon, J. C. Choi and H. L. Park, Appl. Phys. Lett., 2004, 84, 2931.
3 W. B. Im, Y. I. Kim, N. N. Fellows, H. Masui, G. A. Hirata, S. P. Den and B. R. Seshadri, Appl. Phys. Lett., 2008, 93, 091905.
4 Z. Y. Mao and D. Wang, J. Inorg. Chem., 2010, 49, 4922.
5 C. Hecht, F. Stadler, P. J. Schmidt, J. S. A. der Guenne, V. Baumann and W. Schnick, Chem. Mater., 2009, 21, 1595.
6 Z. G. Xia, R. S. Liu, K. W. Huang and V. Drozd, J. Mater. Chem., 2012, 22, 15183.
7 W. Z. Lv, Y. C. Jia, Q. Zhao, M. M. Jiao, B. Q. Shao, W. Lu and H. P. You, Adv. Opt. Mater., 2014, 2, 183.
8 N. Guo, H. You, Y. Song, M. Yang, K. Liu, Y. Zheng Y. Huang and H. Zhang, J. Mater. Chem., 2010, 20, 9061.
9 W. R. Liu, C. H. Huang, C. W. Yeh, J. C. Tsai, Y. C. Chiu, Y. T. Yeh and R. S. Liu, Inorg. Chem., 2012, 51, 9636.
10 W. Lu, Y. C. Jia, Q. Zhao, W. Z. Lv and H. P. You, Chem. Commun., 2014, 50, 2635.
11 N. Guo, H. P. You, C. Z. Jia, R. Z. O. Yang and D. H. Wu, Dalton Trans., 2014, 43, 12373.
12 H. K. Liu, L. B. Liao and Z. G. Xia, RSC Adv., 2014, 4, 7288.
13 J. C. Zhang, Y. Z. Long, H. D. Zhang, B. Sun, W. P. Han and X. Y. Sun, J. Mater. Chem. C, 2014, 2, 312.
14 M.M. Jiao, Y.C.Jia, W. Lu, W.Z. Lü,Q.Zhao, B.Q. Shaoand H. P. You, J. Mater. Chem. C, 2014, 2, 4304.
15 L. Wu, Y.Zhang, M. Gui, P. Lu, L. Zhao, S. Tian, Y. Konga andJ. Xu, J. Mater. Chem., 2012, 22, 6463.
16 S. Zhang, H. Liang and C. Liu, J. Phys. Chem. C, 2013, 117, 2216.
17 D. Kang, H. S. Yoo, S. H. Jung, H. Kim and D. Y. Jeon, J. Phys. Chem. C, 2011, 115, 24334.
18 G. Zhu, S. Xin, Y. Wen, Q. Wang, M. Que and Y. Wang, RSCAdv., 2013, 3, 9311.
19 D. Jia, R. S. Meltzer and W. M. Yen, Appl. Phys. Lett., 2002, 80, 1535.
20 K. A. Denault, Z. Chenga, J. Brgocha, S. P. DenBaars andR. Seshadri, J. Mater. Chem. C, 2013, 1, 7339.
21 G. Zhang, J. Wang, Y. Chen and Q. Su, Opt. Lett., 2010, 35, 2382.
22 M. Jiao, N. Guo, W. Lü, Y. Jia, W. Lv, Q. Zhao, B. Shao andH. You, Inorg. Chem., 2013, 52, 10340.
23 N. Guo, Y. Song, H. You, G. Jia, M. Yang, K. Liu, Y. Zheng, Y. Huang and H. Zhang, Eur. J. Inorg. Chem., 2010, 4636.
24 N. R. J.Poolton, A. J. J.Bos, and P.Dorenbos,J. Phys.: Condens. Matter,2012, 24, 225502.
25J.Y. Wang, Y.l Huang, and Y.D. Li, J. Am. Ceram. Soc., 2011,95,1494.
26 C. Kulshreshtha, S. H. Cho, Y. S. Jung, and K. S. Sohn, J. Electrochem. Soc.,2007,154,J86.
27. K. Uheda, N. Hirosaki, Y. Yamamoto, A. Naito, T. Nakajima, and H. Yamamoto, Electrochem. Solid-StateLett, 2006, 9, H22.
28. H. Watanabe, H. Wada, K. Seki, M. Itou, and N. Kijima, J. Electrochem. Soc., 2008, 155, F31.
29. X. Piao, K. Machida, T. Horikawa, H. Hanzawa, Y. Shimomura, and N. Kijima, Chem. Mater.,2007,19, 4592.
30. Y. Q. Li, C. M. Fang, G. de With, and H. T. Hintzen, J. Solid State Chem.,2004, 171, 4687.
31. Y. Q. Li, G. de With, and H. T. Hintzen, J. Alloy. Comp., 2004, 385, 1–11.
32. R. S. Liu, Y. H. Liu, N. C. Bagkar, and S. F. Hua, Appl. Phys. Lett., 2007, 91, 061119.

33. Y. Q. Li, A. C. A. Delsing, G. de With, and H. T. Hintzen, Chem. Mater., 2005, 17, 3242.
34. T. Suehiro, N. Hirosaki, R. J. Xie, and M. Mitomo, Chem. Mater.,2005, 17, 308–314 (2005).
35. K. Sakuma, N. Hirosaki, R. J. Xie, Y. Yamamoto, and T. Suehiro, Mater. Lett., 2007, 61, 547.
36. R. J. Xie, K. Kimoto, T. Sekiguchi, Y. Yamamoto, T. Suehiro, M. Mitomo, and N. Hirosaki, Appl. Phys.Lett., 2005, 86, 211905.
37. R. J. Xie, Naoto Hirosaki, Science and Technology of Advanced Materials 8, no. 7 (2007): 588-600.
38. Ekstrom, T., Olsson, P.-O., Holmstrom, J. Eur. Ceram. Soc, 1993. 12.165.
39. O. Lindqvist, J. Sjoberg, S. Hull, R. Pompe, ActaCrystallogr B, 1991, 47, 672.
40. H. You, X. Wu, H. Cui and G. Hong, J. Lumin., 2003, 104, 223.
41. Y. Song, N. Guo and H. You, Eur. J. Inorg. Chem., 2011, 2327.
42. N. Guo, Y. Song, H. You, G.Jia, M. Yang, K. Liu, Y. Zheng,Y. Huang and H. Zhang, Eur.J. Inorg. Chem.,2010.4636.
43. Lahoz, F.; Martin, I. R.; Mendez-Ramos, J.; Nunez, P. J. Chem. Phys. 2004, 120, 6180−90.
44. Paulose, P.; Jose, G.; Thomas, V.; Unnikrishnan, N.; Warrier, M. J. Phys. Chem. Solids 2003, 64, 841−846.
45. Kwon, K. H.; Im, W. B.; Jang, H. S.; Yoo, H. S.; Jeon, D. Y. Inorg. Chem. 2009, 48, 11525−32.
46. D. L. Dexter and J. H. Schulman, J. Chem. Phys., 1954, 22, 1063.
47. G. Blasse, Philips Res. Rep. 1969, 24, 131−144.
48. P. L.Li, Z. J. Wang, Z. P. Yang and Q. L. Guo, J. Mater. Chem. C, 2014, 2, 7823.
49. Z.G.Yang, Z.Y. Zhao, M.D. Que, Y.H. Wang, Opt. Mater., 2013, 01, 024.